RESEARCH ARTICLE OPEN ACCESS

Electron-Plasmon Scattering Effect on Electron Transport Properties in ZnO Using an Ensemble Monte Carlo Calculation Including Three-valley Band Structure Model

[1]Sima Eivazi and [2]Hadi Arabshahi
[1]*Central Azad University, Tehran, Iran*
[2]*Department of Physics, Institute of Condensed Theory Matter, Sweden*

ABSTRACT
A Monte Carlo method has been developed for the study of electron transport properties in ZnO taking into account the electron-plasmon scattering effect. It is shown that electron-plasmon scattering affects substantially the hot-electron energy distribution function and transport properties in bulk ZnO. The following scattering mechanisims, i.e, impurity, polar optical phonon, acoustic phonon, piezoelectric are also included in the calculation. Ionized impurity scattering has been treated beyound the Born approximation using the phase-shift analysis.
Keywords: Electron-plasmon; hot-electron; acoustic phonon; ionized impurity

Date of Submission: 25-01-2021 Date of Acceptance: 10-02-2021

I. INTRODUCTION

The problems of high-field transport in semiconductors have been extensively investigated both theoretically and experimentally for many years. Many numerical methods available in the literature (Monte Carlo method, Iterative method, variational method, Relaxation time approximation, or Mattiessen's rule) have lead to approximate solutions to the Boltzmann transport equation [1-4]. The Monte Carlo method has been widely used to study hot-electron problems [5-9]. The principle of this method is to simulate on a computer the motion of one electron in momentum space through a large number of scattering processes taking note of the time that the electron spends in each element of momentum space during its flight, this time being proportional to the distribution function in the elements. The procedure used for the following the motion of an electron requires random numbers to represent the time which the electron drifts before being scattered, and to represent the final state after the scattering event. The probability distribution for these random numbers can be completely specified in terms of the electric field strength and the transition probabilities due to the various scattering processes.

Electrons in bulk material suffer intravalley scattering by polar optical, non-polar optical, acoustic phonons and piezoelectric scattering, intervalley phonons, and ionized impurity scattering.

Acoustic and piezoelectric scattering are assumed elastic and the absorption and emission rates are combined under the equipartition approximation, which is valid for lattice temperatures above 77 K. Elastic ionised impurity scattering is described using the screened Coulomb potential of the Brooks-Herring model.

It is also found that [10] electron-plasmon scattering affects substantially the electron transport properties in polar semiconductors under strong applied electric field, which is close in value to the intervalley transfer threshold field. It is shown [11] using the Monte Carlo simulations that the electron-plasmon scattering is responsible for an increase of magnitude of both threshold electric field and maximum drift velocity. The electron-plasmon scattering rates were calculated [10] within the framework of a well-known random phase approximation. Here, we present more accurate results of a Monte Carlo simulation of hot-electron distribution function and transport characteristics in ZnO with electron-plasmon scattering processes included.

This article is organized as follows. Details of the electron-plasmon scattering and the Monte Carlo simulation are presented in section II, and the results of steady-state transport simulations including electron-plasmon scattering are discussed in section III.

II. MODEL DETAILS AND ELECTRON SCATTERING

Electronic transport in ZnO material under high applied electric field is studied using the ensemble Monte Carlo simulation. The band structure of the material under study is approximated with an analytical formulation using non-parabolic spherical valleys. Though usage of an analytical band structure is questionable at high applied electric field strengths wherein impact ionization can occure, we adopt its usage here for the following reasons. First, due to the large number of compositions examined, it is too computationally expensive to utilize full band models with their concomitant numerically derived scattering mechanisms. Second, we have found that the analytical model well reflects the low field dynamics critical for assessing the carrier mobility. Since we restrict our work here only to high field phenomena, an analytical band structure is satisfactory.

The familiar three-valley Γ-*U*-*K* approximation of the first conduction band has been used for the wurtzite crystal structure of ZnO.

Band edge energies, effective masses and non-parabolicities are derived from empirical pseudopotential calculations.

We assume that all donors are ionized and that the free-electron concentration is equal to the dopant concentration. For each simulation, the motion of ten thousand electron particles are examined, the temperature being set to 300 K, and the doping concentration being set to 10^{22} m^{-3}. In the case of the ellipsoidal, non-parabolic conduction valley model, the usual Herring-Vogt transformation matrices are used to map carrier momenta into spherical valleys when particles are drifted or scattered. Electrons in bulk material suffer intravalley scattering by polar optical,

non-polar optical and acoustic phonons scattering, intervalley phonons, ionized impurity and electron-plasmon scattering. Acoustic scattering is assumed elastic and the absorption and emission rates are combined under the equipartition approximation, which is valid for lattice temperatures above 77 K. Elastic ionized impurity scattering is described using the screened Coulomb potential of the Brooks-Herring model. Band edge energies, effective masses and non-parabolicities are derived from empirical pseudopotential calculations. In the following section different scattering mechanisms will be discussed.

2.1 Deformation potential scattering

The acoustic modes modulate the inter atomic spacing. Consequently, the position of the conduction and valence band edges and the energy band gap will vary with position because of the sensitivity of the band structure to the lattice spacing. The energy change of a band edge due to this mechanism is defined by a deformation potential and the resultant scattering of carriers is called deformation potential scattering. The energy range involved in the case of scattering by acoustic phonons is from zero to $2\hbar vk$, where v is the velocity of sound, since momentum conservation restricts the change of phonon wavevector to between zero and $2k$, where k is the electron wavevector. Typically, the average value of k is of the order of 10^7 cm^{-1} and the velocity of sound in the medium is of the order of 10^5 cms^{-1}. Hence, $2\hbar vk \sim 1$ meV , which is small compared to the thermal energy at room temperature. Therefore, the deformation potential scattering by acoustic modes can be considered as an elastic process except at very low temperature. The deformation potential scattering rate with either phonon emission or absorption for an electron of energy E in a non-parabolic band is given by Fermi's golden rule as [6-7]

$$R_{de}(k) = \frac{\sqrt{2}D_{ac}^2 (m_t^{*2} m_l^*)^{1/2} K_B T}{\pi \rho v^2 \hbar^4} \frac{\sqrt{E(1+\alpha E)}}{(1+2\alpha E)} \left[(1+\alpha E)^2 + 1/3(\alpha E)^2 \right]$$

(1)

where D_{ac} is the acoustic deformation potential, ρ is the
material density and α is the non-parabolicity coefficient. The formula clearly shows that the acoustic scattering increases with temperature.

2.2 Piezoelectric scattering

The second type of electron scattering by acoustic modes occurs when the displacements of the atoms create an electric field through the piezoelectric effect. This can occur in the compound semiconductors such as the III-V and II-VI materials including ZnO, which in fact has a relatively large piezoelectric constant. The piezoelectric scattering rate for an electron of energy E in an isotropic, parabolic band has been discussed by Ridley [12] who included the modification of the Coulomb potential due to free carrier screening. The screened Coulomb potential is written as

$$V(r) = \frac{e^2}{4\pi\varepsilon_0\varepsilon_s} \frac{\exp(-q_0 r)}{r} \qquad (2)$$

where ε_s is the relative dielectric constant of the material and q_0 is the inverse screening length, which under non-degenerate conditions is given by

$$q_0^2 = \frac{ne^2}{\varepsilon_0 \varepsilon_s K_B T}$$

(3)
where n is the electron density. The expression for the scattering rate of an electron in a non-parabolic band structure retaining only the important terms can be written as [6-7]

$$R_{pz}(k) = \frac{\sqrt{m^*}e^2K_{av}^2K_BT}{4\sqrt{2}\pi\hbar^2\varepsilon_0\varepsilon_s}\gamma^{-1/2}(E)(1+2\alpha E)^2 \times \left[\ln(1+\frac{8m^*\gamma(E)}{\hbar^2q_0^2} - \frac{1}{1+\hbar^2q_0^2/8m^*\gamma(E)} + \left(\frac{\sqrt{2}\alpha E}{1+2\alpha E}\right)^2\right]$$

(4)
where K_{av} is the dimensionless so called average electromechanical coupling constant.

2.3 Polar optical phonon scattering

The dipolar electric field arising from the opposite displacement of the negatively and positively charged atoms provides a coupling between the electrons and the lattice which results in electron scattering. This type of scattering is called polar optical phonon scattering and at room temperature is generally the most important scattering mechanism for electrons in III-V semiconductors, and this is also the case in ZnO despite the fact that the optical phonon energy is particularly high at ~ 93 meV which suppresses the phonon population and also electrons must reach that energy before phonon emission is possible. The scattering rate due to this process for an electron of energy E in an isotropic, non-parabolic band is [6-7]

$$R_{po}(k) = \frac{\sqrt{2m^*}e^2\omega_{op}}{8\pi\varepsilon_0\hbar}(\frac{1}{\varepsilon_\infty} - \frac{1}{\varepsilon_s})\frac{1+2\alpha E'}{\gamma^{1/2}(E)} \times F_0(E,E')\{N_{op}, N_{op}+1\}$$

(5)
where

$$F_0(E,E') = C^{-1}\left\{A\ln\left|\frac{\gamma(E)^{1/2}+\gamma(E')^{1/2}}{\gamma(E)^{1/2}-\gamma(E')^{1/2}}\right| + B\right\}$$

$$A = \left[2(1+\alpha E)(1+\alpha E') + \alpha(\gamma+\gamma')\right]^2$$

$$B = -2\alpha\gamma^{1/2}\gamma'^{1/2}\left[4(1+\alpha E)(1+\alpha E') + \alpha(\gamma+\gamma')\right]$$

$$C = 4(1+\alpha E)(1+\alpha E')(1+2\alpha E)(1+2\alpha E')$$

where N_{op} is the phonon occupation number and the upper and lower cases refer to absorption and emission, respectively. For small electric fields, the phonon population will be very close to equilibrium so that the average number of phonons is given by the Bose-Einstein distribution

$$N_{op} = \frac{1}{\exp(\frac{\hbar\omega_{op}}{K_BT}) - 1} \quad (6)$$

where $\hbar\omega_{op}$ is the polar optical phonon energy.

2.4 Non-polar optical phonon scattering

Non-polar optical phonon scattering is similar to deformation potential scattering, in that the deformation of the lattice produces a perturbing potential but in this case the deformation is carried by optical vibrations. The non-polar optical phonon scattering rate in non-parabolic bands is given by [6-7]

$$R_{npo}(k) = \frac{D_{od}^2(m_t^{*2}m_l^*)^{1/2}}{\sqrt{2}\pi\hbar^3\rho\omega_{op}}(1+2\alpha E)\gamma^{1/2}(E)\left[N_{op}, N_{op}+1\right]$$

(7)
where D_{od} is the optical deformation potential and $E = E' \pm \hbar\omega_{op}$ is the final state energy phonon absorption (upper case) and emission (lower case).

2.5 Intravalley impurity scattering

This scattering process arises as a result of the presence of impurities in a semiconductor. The substitution of an impurity atom on a lattice site will perturb the periodic crystal potential and result in scattering of an electron. Since the mass of the impurity greatly exceeds that of an electron and the impurity is bonded to neighboring atoms, this scattering is very close to being elastic. Ionized impurity scattering is dominant at low temperatures because, as the thermal velocity of the electrons decreases, the effect of long-range Coulombic interactions on their motion is increased. The electron scattering by ionized impurity centres has been discussed by Brooks-Herring [13] who included the modification of the Coulomb potential due to free carrier screening. The scattering rate for an isotropic, non-parabolic band structure is given by [6-7]

$$R_{im}(k) = \frac{8\pi n_i e^4}{k_s^2\hbar q_0}(m_t^{*2}m_l^*)^{1/2}\gamma^{1/2}(E)\frac{1+2\alpha E}{1+4\sqrt{2}\gamma(E)(m_t^{*2}m_l^*)^{1/6}/\hbar q_0}$$

(8)

where n_i is the impurity concentration, q_0 is the screening length and k_s is the dielectric constant of the material.

2.6 Intravalley alloy scattering

Alloy scattering refers to the scattering due to the random distribution of the component atoms of the alloy among the available lattice sites. Harrison *et al.* [14] assumed that the alloy crystal potential can be described as a perfectly periodic potential which is then perturbed by the local deviations from this potential, due to the disordering effects in the alloy. Using the Harrison model [14],

the scattering rate due to the chemical disorder in a ternary alloy of electrons in a non-parabolic band is given by [6-7]

$$R_{alloy}(k)=\frac{4\sqrt{2}\pi m^{*3/2}r_0^6}{9\hbar^4}\frac{x(1-x)(\Delta U)^2}{\Omega^2}\gamma^{1/2}(E)(1+2\alpha E)$$
(9)

where x denotes the molar fraction of one of the binary
components of the alloy, Ω is the volume of the primitive cell and ΔU is the spherical scattering potential.

2.7 Intervalley scattering due to optical phonons

The constant energy surfaces for the conduction band of ZnO derive from several valleys. Thus, under the application of high electric field, electrons can be scattered from an initial state in a certain valley to a final state in a non-equivalent valley. For example, in wurtzite ZnO this process occurs when an electron in the Γ valley is heated and is able to transfer to the higher *U* and *K* valleys. In the case of Γ to zone edge valley scattering the process involves a substantial change of electron wavevector. Acoustic and optical phonons of sufficiently large wavevector can effect the transition but in view of the large wavevectors involved it is normal to treat all processes like deformation scattering by optical phonons. Then the total nonequivalent intervalley scattering rate from a state k in a certain valley to a set of Z_f different valleys is given by [6-7]

$$R_{equiv}(k)=\frac{(D_tK)_i^2 Z_f(m_t^{*2}m_l^*)^{1/2}}{\sqrt{2}\pi\rho\omega_{op}\hbar^3}(\varepsilon\pm\hbar\omega_{op}-\Delta\varepsilon_{fi})^{1/2}\times$$
$$\left[1+2\alpha(\varepsilon\pm\hbar\omega_{op}-\Delta\varepsilon_{fi})\right]\left\{N_{op,}N_{op}+1\right\}$$
(10)

where $\hbar\omega_{op}$ is the optical phonon energy and $\Delta\varepsilon_{fi}$ is the difference between the energies of the bottoms of the final and initial valleys. $(D_tK)_i$ is the coupling constant, which depends on the initial and final valleys and the branch of phonons involved in the transition. N_{op} is the phonon occupation number, with the upper and lower cases corresponding to phonon absorption and emission, respectively.

2.8 Electron-plasmon scattering

The electron-plasmon interaction Hamiltonian can be written in random phase approximation as [15]

$$H_{\text{int}}=\sum M_q(a_q c_{k+q}^{+}c_k+a_{-q}^{+}c_{k+q}^{+}c_k)$$
(11)

Here a_q^+, a_q and c_k^+, c_k are the creation and annihilation operators for plasmons and electrons, respectively. The matrix element

$$M_q=\sqrt{\frac{e^2\hbar^3}{8\Omega\varepsilon m^{*2}\omega_p(q)}}.(2qk+q^2)/q$$
(12)

where $\omega_p(q)$ is the dispersion relation for plasmons, q and k are the plasmon and electron momenta, respectively, e and m^* are the charge and effective mass of an electron, ε the background dielectric constant, and Ω the real-space volume. The first term in parentheses in equation 11 describes the plasmon absorption process which obeys the energy conservation law as

$$\varepsilon_{k+q}-\varepsilon_k=\hbar\omega_p(q)\geq 0$$
(13)

where ε_k is the energy of electron with momentum k. In a similar manner, the plasmon emission process, in accordance with the second term in parentheses in equation 11, is governed by the energy conservation law which can be written as

$$\varepsilon_k-\varepsilon_{k+q}=\hbar\omega_p(q)\geq 0$$
(14)

Note that equation 14 describes the emission of plasmon with momentum $-q$. To impart a more conventional form to the energy conservation law, repalce the variable of summation q in terms governing the plasmon emission in equation 1 by $-q$. Then we can rewrite equation 11 as

$$H_{\text{int}}=\sum(M_q a_q c_{k+q}^{+}c_k+M_{-q}a_q^{+}c_{k-q}^{+}c_k)$$
(15)

The notation of equation 11 leads to the following form of the energy conservation law for the emission processes

$$\varepsilon_k-\varepsilon_{k-q}=\hbar\omega_p(q)\geq 0$$
(16)

From the Fermi Golden rule, we can calculate the electron-plasmon scattering rates for emission W_e and absorption W_a

$$W_{e,a}(k)=\frac{2\pi}{\hbar}\int\frac{\Omega dq}{8\pi^3}\left|\langle f|H_{\text{int}}|i\rangle\right|^2\times\delta\left[\varepsilon_{k'}-\varepsilon_k\pm\hbar\omega_p(q)\right]$$
(17)

where k and k' are electron momenta in an initial state $|i\rangle$ and a final state $|f\rangle$, respectively. Here and further the upper signs in formulae correspond to the plasmon emission, whereas the lower ones do to the plasmon absorption. By using equation 11 and the energy conservation requirements in the forms of equations 13 and 15 which are consistent with this notation of H_{int}, equation 17 becomes

$$W_{e,a}(k)=\frac{2\pi}{\hbar}\int\frac{\Omega dq}{8\pi^3}M_{\mp q}^2\delta\left[\varepsilon_{k\mp q}-\varepsilon_k\pm\hbar\omega_p(q)\right]\times\left\{(N_q+1)_{em};(N_q)_{ab}\right\}$$
(18)

where N_q is the Bose-Einstein distribution fuction for plasmons. The integration bounds with respect to q are defined from the following conditions

$$\omega_p(q)\le\hbar kq/m^*\mp\hbar q^2/2m^*$$
$$\omega_p(q)\ge\hbar k_f q/m^*+\hbar q^2/2m^*$$
(19)

where k_f is the electron momentum at the Fermi surface.

III. CALCULATED RESULTS

The electron-plasmon scattering is included only in the low effective mass Γ valley. So, we have just taken into account the electric field dependence of the electron concentration in the Γ valley, which arises due to the intervalley electron transfer, when calculating the plasmon frequency in the Γ valley. The effect of the electron-plasmon scattering on the steady-state electron distribution function is shown in figure 1. As it is seen, the inclusion of the electron-plasmon scattering leads to the effective cooling of the hot-electron system.

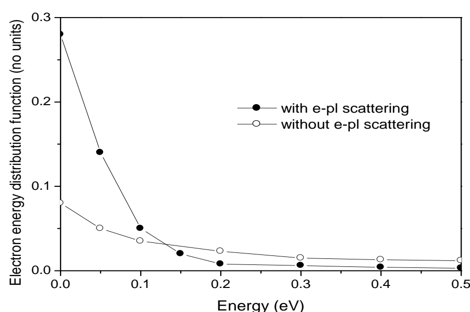

Fig. 1. Electron energy distribution function f(ε) for electric field strength of 10 KV/cm with the electron-plasmon scattering included and without the electron-plasmon scattering at room temperature.

In figure 2 the plasmon emission and absorption rates are shown as functions of the electron energy. As it can be seen, the plasmon scattering occurs when the initial electron energy exceeds the threshold energy. At this threshold energy the electron-plasmon scattering rates with emission and absorption of plasmons rise sharply up to 1.7×10^{14} and 1.3×10^{14} s^{-1}, respectively and then reduces slowly for higher energy. This result shows the importance of electron-plasmon scattering on electron transport properties in ZnO material.

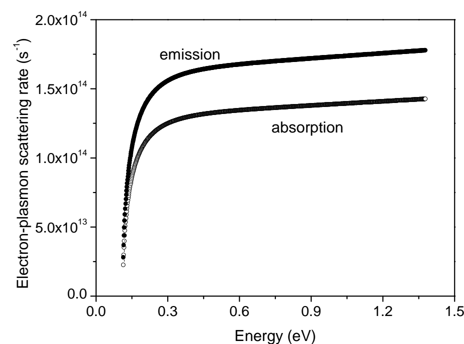

Fig. 2. Electron-plasmon scattering rates with emission and absorption of plasmons as a functions of the electron energy at room temperature.

Figure 3 depicts the mean electron drift velocity as a function of the steady electric field. As it can be seen, the electron-plasmon causes the threshold electric field to rise since the process of increasing the energy of electrons to transfer to the upper valleys is hindered as it is clear in figure 4. At the same time, electron momentum scattering happens predominantly at small scattering angles thereby resulting in a higher electron drift velocity. From figure 3, it follows that the electron-plasmon scattering in the central Γ valley substantially affects the transport properties in ZnO, the threshold electric field and maximum electron drift velocity increase by %30 and %17, respectively, and Ohmic mobility drops by %15.

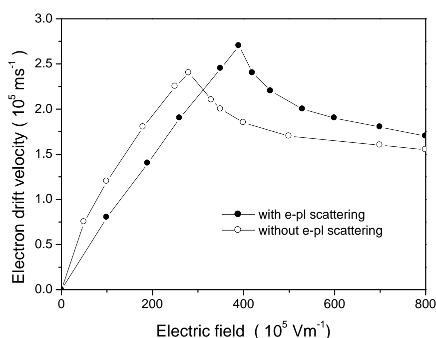

Fig. 3. Calculated electron steady-state drift velocity in bulk ZnO
as a function of applied electric field assuming a donor concentration of 10^{22} m^{-3} for the electron-plasmon scattering included and without the electron-plasmon scattering at room temperature.

In figure 5, the relative Γ valley electron population is shown as a function of the electric field. It is seen that the electron population in the central Γ valley increases with including electron-plasmon scattering.

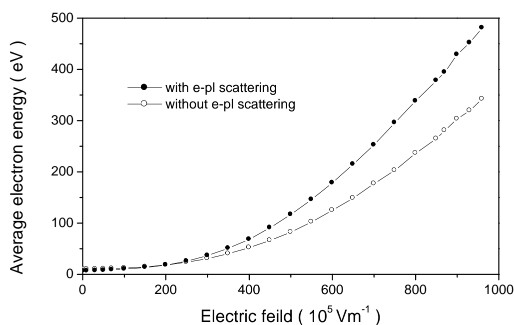

Fig. 4. Average electron kinetic energy as a function of applied electric field in bulk ZnO for the electron-plasmon scattering included and without the electron-plasmon scattering at room temperature.

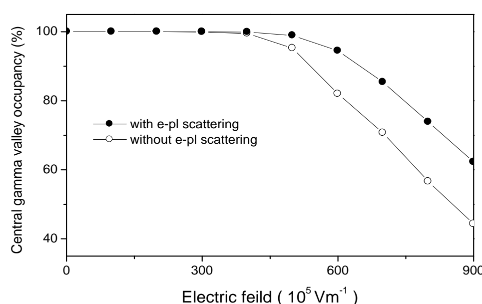

Fig. 5. Central Γ valley occupancy as a function of applied electric field in bulk ZnO for the electron-plasmon scattering included and without the electron-plasmon scattering at room temperature.

IV. CONCLUSION

Using an ensemble Monte Carlo method, it was shown that the electron-plasmon scattering in the Γ valley substantially affects the hot-electron energy distribution function and transport properties in ZnO. It is shown that the threshold electric field and maximum drift velocity increase by %30 and %17, respectively, and Ohmic mobility drops by %15. This is caused by combined effects of effective cooling of electron gas by electron-plasmon scattering and predominantly forward peaked momentum relaxation for all electron momenta.

REFERENCES

[1]. K. Tomizawa, Numerical Simulation of Submicron Semiconductor Devices. Artech House. London, Boston, (1993)
[2]. K. Blotekjaer, IEEE Trans. Electron Dev. **17** 38 (1970)
[3]. C. L. Gardner, IEEE Trans. Electron Dev. **38** 392 (1991)
[4]. Y. K. Feng and A. Hintz, IEEE Trans. Electron Dev. **35** 1419 (1988)
[5]. M. A. Alsunaidi, S. M. Hammadi and S. M. El-Ghazaly, Int. J. Num. Mod.: Newt. Dev. Fields. **10** 107 (1997)
[6]. C. Moglestue, Monte Carlo Simulation of Semiconductor Devices, 1993, Chapman and Hall
[7]. C. Jacoboni and P. Lugli, The Monte Carlo Method for semiconductor and Device Simulation, 1989, Springer-Verlag
[8]. H. Arabshahi, M. R. Benam and B. Salahi Modern Physics Letters B. **21**, 1715 (2007)
[9]. H. Arabshahi, Modern Physics Letters B. **21**, 199 (2007)
[10]. K. Di. and K. Brennan, J. Appl. Phys. **69**, 3097 (1991)
[11]. N. Mansour, K. Di. and K. Brennan, J. Appl. Phys. **70**, 6854 (1991)
[12]. B. K. Ridley, Electrons and phonons in semiconductor multilayers, Cambridge University Press (1997)
[13]. D. Chattopadhyay and H. J. Queisser, Review of Modern Physics, **53**, part1 (1981)
[14]. J. W. Harrison and J. R. Hauser, Phys. Rev. B, **13**, 5347 (1976)
[15]. O. Madelung, Introduction to Solid State Theory, Springer, Heidelberg, (1978)

Hadi Arabshahi received the B. S degree in physics from the Ferdowsi University of Mashhad, Iran, in 1992 and the Ph. D. degree in computational physics from Durham University, United Kingdom, in 2002. Right after graduation, in summer 2002, he joined the physics department, University of Mashahd. He has published over 185 peer-reviewed journal papers and contributed to more than 30 conference papers and presentations. His research activities include semiconductor device simulations, high field transport properties in bulk and devices, transient relaxation in materials and devices, simulation of optoelectronic devices, electronics properties of low-dimensional and curved nanostructures and quantum information.

Sima Eivazi received the B. Sc degree in communicational science from the centeral Azad university, Tehran, Iran in 2014. Her research involves modeling of materials characteristics.